Pure appl. geophys. 159 (2002) 449–471
0033–4553/02/030449–23 $ 1.50 + 0.20/0

Pure and Applied Geophysics

Application of Kalman Filtering Techniques for Microseismic Event Detection

ERICK BAZIW[1] and IAIN WEIR-JONES[1]

Abstract — Microseismic monitoring systems are generally installed in areas of induced seismicity caused by human activity. Induced seismicity results from changes in the state of stress which may occur as a result of excavation within the rock mass in mining (i.e., rockbursts), and changes in hydrostatic pressures and rock temperatures (e.g., during fluid injection or extraction) in oil exploitation, dam construction or fluid disposal. Microseismic monitoring systems determine event locations and important source parameters such as attenuation, seismic moment, source radius, static stress drop, peak particle velocity and seismic energy. An essential part of the operation of a microseismic monitoring system is the reliable detection of microseismic events. In the absence of reliable, automated picking techniques, operators rely upon manual picking. This is time-consuming, costly and, in the presence of background noise, very prone to error. The techniques described in this paper not only permit the reliable identification of events in cluttered signal environments they have also enabled the authors to develop reliable automated event picking procedures. This opens the way to use microseismic monitoring as a cost-effective production/operations procedure. It has been the experience of the authors that in certain noisy environments, the seismic monitoring system may trigger on and subsequently acquire substantial quantities of erroneous data, due to the high energy content of the ambient noise. Digital filtering techniques need to be applied on the microseismic data so that the ambient noise is removed and event detection simplified. The monitoring of seismic acoustic emissions is a continuous, real-time process and it is desirable to implement digital filters which can also be designed in the time domain and in real-time such as the Kalman Filter. This paper presents a real-time Kalman Filter which removes the statistically describable background noise from the recorded seismic traces.

Key words: Microseismic monitoring, Kalman Filter, state-space, automated event detection, ambient noise.

1. Introduction

Microseismic monitoring systems are used in mining rock mechanics, civil construction, petroleum extraction, and heavy structural engineering. Extreme examples of energy release can cause violent rockbursts which result in fatalities and injuries among underground personnel and damage to mine structures (e.g., drifts, stopes, shafts, etc.). Microseismic systems are capable of detecting rock failures in the

[1] Weir-Jones Engineering Consultants Ltd., 2040 West 10th Ave., Vancouver, B.C. Canada, V6J 2B3. E-mail: wjgroup@weir-jones.com

vicinity of underground excavations caused by the sudden release of strain energy resulting from the redistribution of stresses around openings.

Various hydrocarbon production sites also benefit from seismic monitoring systems during certain phases of production. Primary or secondary extraction or the injection of material into the reservoir to enhance production can cause significant stress changes. These stress changes can result in failures of the overlying strata and the migration of hydrocarbons to aquifers or to the ground surface. Thus microseismic monitoring can be used to satisfy environmental concerns, meet regulatory requirements and assess the development of induced fracturing within the reservoir. In addition, the microseismic monitoring systems have been successful in identifying and locating casing failures due to steam stimulation in oil sands (TALEBI *et al.*, 1998).

During filling of hydroelectric or large irrigation reservoirs, changes in regional loading and pore pressures cause significant stress variations within the surrounding rock mass. These can induce a wide range of micro- and macroseismic events, some of which are capable of causing damage to adjacent structures or to the dam itself. Microseismic monitoring can locate and characterize these potentially hazardous induced events.

Irrespective of the cause of microseismic events, their reliable detection and placement on a common time base is of critical importance. This is because the arrival times of wavelets at various detector packages within a three-dimensional array provide the basis for the calculation of the location of the microseismic event. Imprecision or uncertainty in arrival time determination reduces the precision of the source location operation. In many microseismic monitoring situations – for example where there is interest in the behaviour of specific geological features or where events must be related to specific structures in a mining or hydrocarbon extraction environment – the accurate determination of event arrival times is the primary rationale for the installation of the system. Hence, techniques such as the one described in this paper open the way for the more widespread use of microseismic monitoring in a number of industrial applications.

The environmental and seismic models used in this paper are designed to fit into a Kalman Filter (KF) formulation. The Kalman Filter is an optimal (in a least-squares sense) recursive filter which is based on state-space, time-domain formulation of physical problems, thereby avoiding difficulties commonly associated with frequency domain filters (BAZIW, 1993), and which is ideal for real-time applications. The KF requires that the physical problem be modelled by a set of first-order differential equations which, with initial conditions, uniquely define the system behaviour. The filter utilizes a knowledge of system and measurement errors and statistical information about the initial conditions (BAZIW, 1988). Section 2 presents the KF microseismic event detection formulation.

The performance of the KF presented in this paper was first evaluated by generating synthetic source wavelets which have correlated earth noise added.

Section 3 presents results from the seismic data simulation and processed real data obtained from a heavy oil extraction facility in Northern Canada.

2. Kalman Filter Formulation

The Kalman Filter is an optimal (least-squares) recursive filter which is based on state-space, time-domain formulations of physical problems. Application of this filter requires that the physical problem be modified by a set of first-order differential equations which, with initial conditions, uniquely define the system behaviour. The filter utilizes knowledge of system and measurement dynamics, assumed statistics of system noises and measurement errors and statistical information regarding the initial conditions. Figure 1 illustrates the essential relation between the system, the measurements and the Kalman Filter.

Figure 1 indicates the scope of information the KF takes into account. As can be seen, the statistics of the measurement and state errors are essential components of the filter. The *a priori* information provides for optimal use of any number, combination and sequence of external measurements. The KF can be applied to problems with linear time-varying systems and with non-stationary system and measurement statistics. Problems with nonlinearities can be handled by linearizing the system and measurement equations. The Kalman Filter is readily applied to estimation, smoothing and prediction.

From the published technical literature, it seems that geophysical data processing has been primarily carried out by the application of frequency domain and steady-state filters such as the Weiner Filter (KANASEWICH, 1981). These filters put many restrictions on the structure of the problem. In general, one assumes non-time-varying system equations (where the coefficients of the system differential equation are constant), and statistically stationary error processes (GELB, 1978).

If the geophysical problem can be structured into one susceptible to the application of the Kalman Filter, it is possible that better state and system

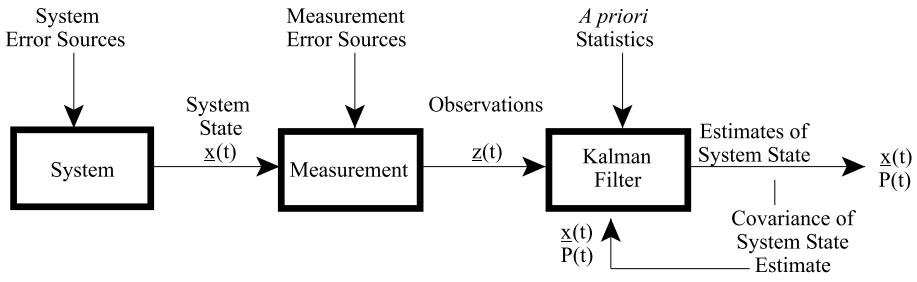

Figure 1
Block diagram of system, measurement, and Kalman Filter.

parameters would be obtained as compared to those derived from use of the frequency domain and steady-state filters. In addition, the KF is ideally suited for real-time optimal data filtering in situations where each new measurement provides for an updated state estimate. This feature of the KF is particularly useful for microseismic event detection. Another advantage of a Kalman Filter is that it allows one to use "state noise" to compensate for errors in the mathematical model. The use of state noise causes the filter to apply less weight to measurements made in the distant past, and to apply more weight to state vector estimates based on more recent measurement data.

BAYLESS and BRIGHAM (1970) were among the first researchers to fit geophysical problems into the Kalman Filter formulation. In addition, MENDEL (1983, 1995) has carried out extensive work in fitting geophysical problems into state-space representations.

2.1 Standard Kalman Filter Governing Equations

The KF is a method for estimating a state vector $\underline{x}$ from measurement $\underline{z}$. The state vector may be corrupted by a noise vector $\underline{w}$ and the measurement vector is corrupted by a noise vector $\underline{v}$. The KF filter is applicable for systems that can be described by a first-order differential equation in $\underline{x}$ and a linear (matrix) equation in $\underline{z}$. The KF can be described in both continuous and discrete form. The continuous state and measurement equations are given by

$$\dot{\underline{x}}(t) = F(t)\underline{x}(t) + G(t)\underline{w}(t) \tag{1}$$

$$\underline{z}(t) = H(t)\underline{x}(t) + \underline{v}(t) \tag{2}$$

where $\underline{x}$ is an n-vector, $\underline{w}$ is a p-vector, and $\underline{z}$ and $\underline{v}$ are m-vectors.

The random (vector) processes $\underline{w}$ and $\underline{v}$ are assumed to be zero mean, white noise processes, so that

$$\begin{aligned} &E[\underline{w}(t)] = \underline{0} \quad \text{and} \quad E[\underline{v}(t)] = \underline{0}, \\ &E\left[\underline{w}(t)\underline{w}(\tau)^T\right] = Q(t)\delta(t-\tau), \\ &E\left[\underline{v}(t)\underline{v}(\tau)^T\right] = R(t)\delta(t-\tau). \end{aligned} \tag{3}$$

It is further assumed that $\underline{w}$ and $\underline{v}$ are statistically independent of each other, so that

$$E\left[\underline{w}(t)\underline{v}(\tau)^T\right] = \underline{0} \tag{4}$$

In the above equations the superscript T denotes the vector transpose, the E denotes the expected value operation and $\delta(t-\tau)$ is the Dirac delta function.

We use the notation $\hat{\underline{x}}(t'|t)$ to denote an estimate of the state at a time $t', t' \geq t_0$, based on measurements $\underline{z}(\tau)$ on the interval $t_0 \leq \tau \leq t$. It is convenient to make the following definitions:

Definition:
1. If $t' \geq t, \underline{\hat{x}}(t'|t)$ is a *predicted estimate*.
2. If $t' = t, \underline{\hat{x}}(t'|t)$ is a *filtered estimate*.
3. If $t' < t, \underline{\hat{x}}(t'|t)$ is a *smoothed estimate*.

The *estimation error* is defined as

$$\underline{\tilde{x}}(t'|t) \equiv \underline{x}(t') - \underline{\hat{x}}(t'|t) \tag{5a}$$

and the *performance index* of the estimation is given by

$$I[\underline{\tilde{x}}(t'|t)] = E\left[\underline{\tilde{x}}(t'|t)\underline{\tilde{x}}(t'|t)^T\right]. \tag{5b}$$

The estimation problem can now be stated as follows:

Estimation Problem: Given the system defined by eqs. (1) and (2) with statistics defined by (3) and (4), and measurements z(τ) over the interval $t_0 \leq \tau \leq t$, determine an estimate of $\underline{\hat{x}}(t'|t)$ such that $I[\underline{\hat{x}}(t'|t)]$ is minimized.

The solution to this problem is specified by the following equations for the filtered estimate:

State Estimation equation

$$\dot{\underline{\hat{x}}}(t) = F(t)\underline{\hat{x}}(t) + K(t)[\underline{z}(t) - H(t)\underline{\hat{x}}(t)], \tag{6}$$

with

$$\underline{\hat{x}}(t_0) = \underline{\hat{x}}_0$$

given

Kalman Gain matrix

$$K(t) = P(t)H(t)^T R(t)^{-1} \tag{7}$$

Estimation Error Covariance (Matrix Ricatti) equation

$$\dot{P}(t) = F(t)P(t) + P(t)F(t)^T + G(t)Q(t)G(t)^T - K(t)R(t)K(t)^T, \tag{8}$$

with

$$P(t_0) = P_0$$

given.

The error covariance matrix is a positive semi-definite symmetric matrix. A block diagram of the system, measurement and filtered estimates is shown in Figure 1.

Using the notation of GELB (1978), the corresponding discrete state and measurement equations are given by

$$\underline{x}_k = \Phi_{k-1}\underline{x}_{k-1} + \underline{w}_{k-1}, \quad \underline{w}_k \approx N(\underline{0}, Q_k) \tag{9}$$

$$\underline{z}_k = H_k\underline{x}_k + \underline{v}_k, \quad \underline{v}_k \approx N(\underline{0}, R_k). \tag{10}$$

In eqs. (9) and (10), symbol N denotes a normal distribution with mean $\underline{0}$ and variance Q_k and R_k, respectively. The discrete Kalman Filter estimation equations are outlined as follows:

State Estimate Extrapolation:

$$\underline{\hat{x}}_k(-) = \Phi_{k-1}\underline{\hat{x}}_{k-1}(+) \tag{11}$$

Error Covariance Extrapolation:

$$P_k(-) = \Phi_{k-1}P_{k-1}(+)\Phi_{k-1}^T + Q_{k-1} \tag{12}$$

State Estimate Update:

$$\underline{\hat{x}}_k(+) = \underline{\hat{x}}_k(-) + K_k[\underline{z}_k - H_k\underline{\hat{x}}_k(-)] \tag{13}$$

Error Covariance Update:

$$P_k(+) = [I - K_kH_k]P_k(-). \tag{14}$$

I is the identity matrix in eq. (14).

Kalman Gain Matrix:

$$K_k = P_k(-)H_k^T\left[H_kP_k(-)H_k^T + R_k\right]^{-1} \tag{15}$$

Initial Conditions:

$$E[\underline{x}_0] = \underline{\hat{x}}_0, \quad E\left[(\underline{x}_0 - \underline{\hat{x}}_0)(\underline{x}_0 - \underline{\hat{x}}_0)^T\right] = P_0. \tag{16}$$

The computational sequence for the discrete KF is outlined as follows:

A. At time index $k = 0$, specify initial conditions $\underline{\hat{x}}_0$, and P_0, and compute Φ_0 and Q_0.

B. At time index $k = 1$, compute $\underline{\hat{x}}_1(-), P_1(-), H_1, R_1$, and the gain matrix K_1

C. Using the measurement $\underline{z}_1$ at time index $k = 1$, the best estimate of the state at $k = 1$ is given by

$$\hat{x}_1(+) = \hat{x}_1(-) + K_1[z_1 - H_1\hat{x}_1(-)]$$

D. Update the error covariance matrix $P_1(+)$

E. At time index $k = 2$, a new measurement $\underline{z}_2$ is obtained and the computational cycle is repeated.

2.2 Microseismic Event Detection Kalman Filter

As was stated previously, the most important factor when applying the KF is that the physical problem must be modelled/approximated by a set of first-order differential equations. In addition, the statistical properties of the system and measurements need to be modelled such that they can be completely specified by first- and second-order statistics (i.e., expected values and covariances).

The microseismic seismic time series is typically comprised of ambient noise and seismic *P* waves and *S* waves. The first step in defining the Microseismic Event Detection Kalman Filter (MEDKF) is to provide a mathematical description of the ambient background noise.

2.2.1 MEDKF ambient noise model

The authors calculated the autocorrelation and power spectrum of a large number of microseismic ambient noise time series. From these results, it was possible to identify a mathematical model which sufficiently fits the seismic noise processes. Figure 2 illustrates the autocorrelation function and power spectral density of

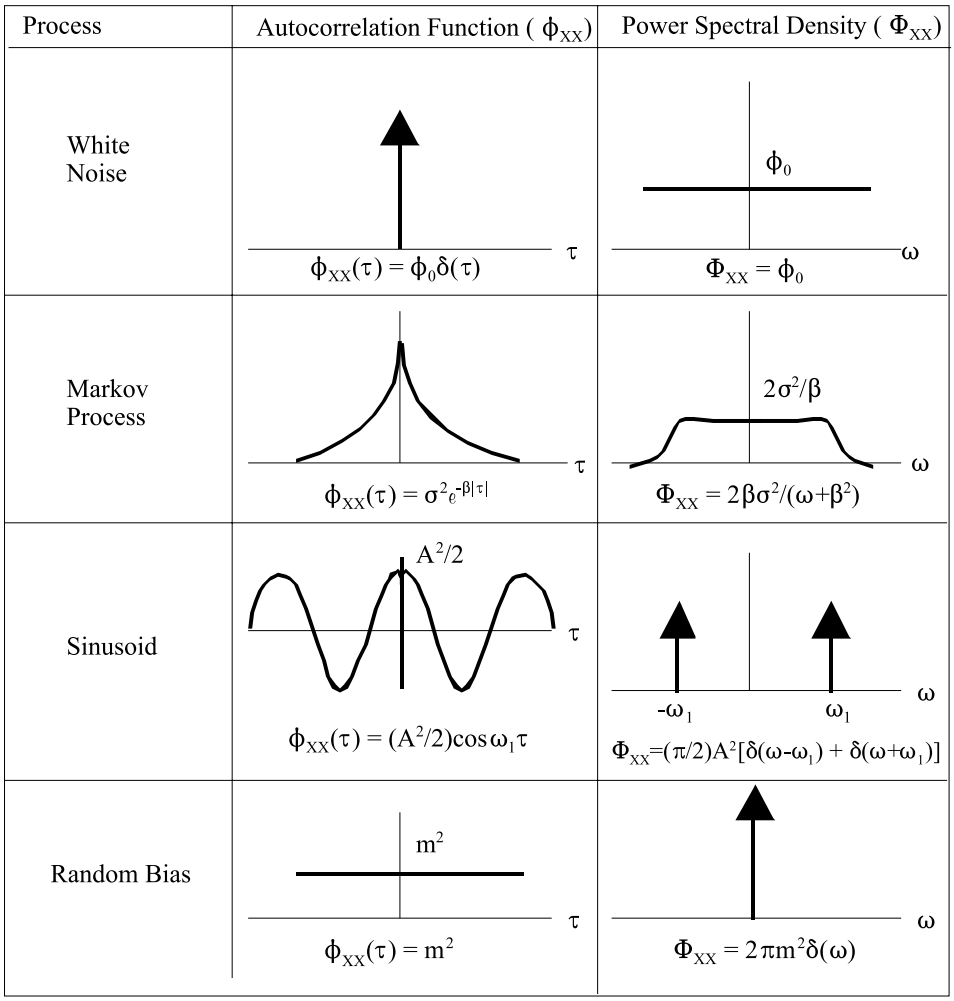

Figure 2
Descriptions of Common Random Processes (GELB, 1978).

common random processes (GELB, 1978). A Gauss-Markov process can be used to describe many physical phenomena (BAZIW, 1994) and is a good candidate to model the microseismic environmental noise.

The Gauss-Markov Process has a relatively simple mathematical description. As in the case of all stationary Gaussian processes, specification of the process autocorrelation completely defines the process. The variance, σ^2, and time constant, T_c (i.e., $\beta = 1/T_c$), define the first-order Gauss-Markov process. These parameters can be derived from the seismic time series by windowing on the noise portion of the trace and calculating the autocorrelation of the ambient noises. A Gauss-Markov process, $n(t)$, has an autocorrelation function defined as follows

$$\phi_{nn}(\tau) = \sigma^2 e^{-\beta|\tau|} \quad . \tag{17}$$

The power spectrum for this autocorrelation function is given by

$$\Phi_{nn}(s) = \frac{2\sigma^2\beta}{-s^2 + \beta^2} \quad . \tag{18}$$

In eq. (18), s is the Laplacian variable. From basic statistical properties, $n(t)$ can be assumed to be generated by passing Gaussian white noise through a linear system transfer function $\sqrt{(2\sigma^2\beta)/(s+\beta)}$; thus for the continuous system we have

$$\dot{n}(t) = -\beta n(t) + \sqrt{2\sigma^2\beta.w(t)} \tag{19}$$

with

$$E[w(t)w(\tau)] = \delta(t-\tau) \quad .$$

To obtain the discrete form for eq. (19), we assume a sampling interval Δ and then solve eq. (19) over this interval. Since β is a constant, the discrete model for the Gauss-Markov process can be written as

$$\begin{aligned} &n_{k+1} = a_w n_k + b_w w_k \\ &where, a_w = e^{-\beta\Delta} \text{ and } b_w = \sigma\sqrt{(1 - e^{-2\beta\Delta})} \end{aligned} \tag{20}$$

In eq. (20), w_k is a zero-mean, timewise-uncorrelated, unit-variance sequence with a Gaussian probability distribution function. n_k is therefore a zero-mean, exponentially-correlated random variable whose standard deviation is σ. The constant a_w can range in values from -1 to $+1$. For a stable variable, we restrict a_w to values between 0 and $+1$. For $a_w \to 0, n(t)$ changes rapidly and tends to be uncorrelated from sample to sample. For $a_w \to 1$, the behaviour of $n(t)$ becomes more sluggish and it tends to change little from sample to sample (LEAR, 1985).

2.2.2 MEDKF seismic wavelet model

The next step in defining the MEDKF system model is fitting the wavelet into a linear mathematical model. A seismic wavelet is typically modelled as an exponentially decaying cyclic waveform (SHERIFF and GELDART, 1982) as follows:

$$A(t) = A_0 e^{-h(t-t_0)} \sin[\omega(t-t_0)], \quad t \geq t_0 \ . \tag{21}$$

In eq. (21) $A_0 \equiv$ initial amplitude, $h \equiv$ damping factor, and $\omega \equiv$ dominant angular frequency (i.e., $\omega = 2\pi f$). The shot noise characteristics of the seismic wavelet make it challenging to model it in the time domain without introducing nonlinearities in the describing equations. We know that the wavelet will take on the form defined in eq. (21), but we do not know at what time (i.e., t_0) it will occur.

To simplify the mathematics and keep the KF in a linear form, we have modelled the seismic wavelet as a periodic process with a random walk amplitude. This process is defined as follows:

$$x_1(t) = x_2(t) \sin[\omega(t-t_0)], \quad t \geq t_0 \ . \tag{22}$$

In eq. (22), $x_1(t)$ is an approximation to the seismic wavelet defined by eq. (21), and $x_2(t)$ is the random walk process approximating A_0 in eq. (21). The random walk process facilitates the provision of some flexibility to the MEDKF when determining the arrival time and initial amplitude (i.e., t_0 and A_0 in eq. (21)) of the seismic wavelet understudy. The random walk process results when uncorrelated signals are integrated. The process is defined as its derivative being driven by white noise as follows:

$$\dot{x}_2(t) = w(t), \quad \text{where} \quad E[w(t)w(\tau)] = q(t)\delta(t-\tau) \ . \tag{23}$$

By using a random walk process to define the seismic wavelets amplitude, we are able to account for arrival time variations and maintain linearity in the KF formulation. The linear continuous differential equation (i.e., eq. (1)) defining the seismic wavelets is outlined as follows:

$$\dot{x}_1(t) = \omega \, x_2(t) \cos(\omega t) \tag{24a}$$

$$\dot{x}_2(t) = w(t), \quad \text{where } E[w(t)w(\tau)] = q(t)\delta(t-\tau) \ . \tag{24b}$$

In eq. (24a) it is assumed that $t_0 = 0$ with respect to eq. (22). In addition, it is also assumed that $x_2(t)$ is a constant when differentiating eq. (22) to obtain eq. (24a) (i.e., $F(t)\underline{x}(t)$ term in eq. (1)). The noise component of the system equation (i.e., $G(t)\underline{w}(t)$ in eq. (1)) handles the random walk term $\dot{x}_2(t) = w(t)$.

2.2.3 MEDKF governing equations

Substituting eqs. (19) and (24) into eq. (1) results in the continuous MEDKF matrix system equation defined as follows:

$$\begin{bmatrix} \dot{x}_1(t) \\ \dot{x}_2(t) \\ \dot{x}_3(t) \end{bmatrix} = \underbrace{\begin{bmatrix} 0 & \omega\cos(\omega t) & 0 \\ 0 & 0 & 0 \\ 0 & 0 & -\beta \end{bmatrix}}_{=F(t)} \begin{bmatrix} x_1(t) \\ x_2(t) \\ x_3(t) \end{bmatrix} + \underbrace{\begin{bmatrix} 0 & 0 \\ q(t) & 0 \\ 0 & \sqrt{2\sigma^2\beta} \end{bmatrix}}_{=G(t)} \begin{bmatrix} w_1(t) \\ w_2(t) \end{bmatrix} . \tag{25}$$

In eq. (25), $E[w_1(t)w_1(\tau)] = \delta(t-\tau)$ and $E[w_2(t)w_2(\tau)] = \delta(t-\tau)$. Both $w_1(t)$ and $w_2(t)$ are Gaussian white noise processes with mean zero and unity variance.

The discrete form of eq. (25) is given as

$$\begin{bmatrix} x_{1(k)} \\ x_{2(k)} \\ x_{3(k)} \end{bmatrix} = \underbrace{\begin{bmatrix} 1 & \Delta\omega\cos[\omega\Delta(k-1)] & 0 \\ 0 & 1 & 0 \\ 0 & 0 & e^{-\beta\Delta} \end{bmatrix}}_{=\Phi_{k-1}} \begin{bmatrix} x_{1(k-1)} \\ x_{2(k-1)} \\ x_{3(k-1)} \end{bmatrix} + \underbrace{\begin{bmatrix} 0 & 0 \\ q_{(k-1)} & 0 \\ 0 & \sigma\sqrt{1-e^{-2\beta\Delta}} \end{bmatrix}}_{=Q_{k-1}} \begin{bmatrix} w_{1(k-1)} \\ w_{2(k-1)} \end{bmatrix} . \tag{26}$$

In eq. (26) Δ is the sampling rate, $q(k-1) = q(t)\Delta$, and $w_{1(k-1)}$ and $w_{2(k-1)}$ are zero mean, unity variance, Gaussian white noise processes.

There is only one scalar measurement available for the MEDKF, which is a combination of both the seismic wavelet understudy and the ambient noise (i.e., $z_k = x_{1(k)} + x_{3(k)}$). This results in the following measurement matrix:

$$H_k = [1 \quad 0 \quad 1] . \tag{27}$$

Given a sequence of measurements $z_0, z_1, \ldots, z_k$, the *observability condition* defines our ability to determine $x_0, x_1, \ldots, x_k$ from the measurements. An observability check was carried out on the previously defined MEDKF formulation and it was found that the MEDKF was completely observable.

3. Results

3.1 Data Simulation

Prior to implementing the previously outlined KF formulation on real data, extensive testing was carried out on synthetic data. This section presents a portion of the test bed results. The first step in the simulation was to outline the source wavelets defined by eq. (21). The *P* wave was modelled with a frequency of 200 Hz, initial amplitude of 160 mm/s^2 and damping factor of 79/s. The *S* wave was modelled with a frequency of 70 Hz, initial amplitude of 200 mm/s^2 and damping factor of 50/s. The sampling rate was set at 0.05 ms and a total sampling time of 1 s was specified. Figure 3 illustrates the source wavelets generated with previous parameters specified.

The next step in data simulation was to specify different Gauss-Markov ambient noise processes. Figure 4 illustrates simulation results when the wavelets shown in Figure 3 have added ambient Gauss-Markov background noise superimposed. Plots a to e in Figure 4 have the following Gauss-Markov parameters specified:

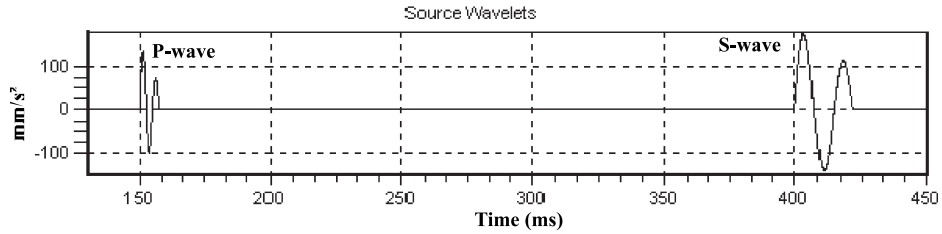

Figure 3
Simulating P and S wavelets by implementing eq. (21).

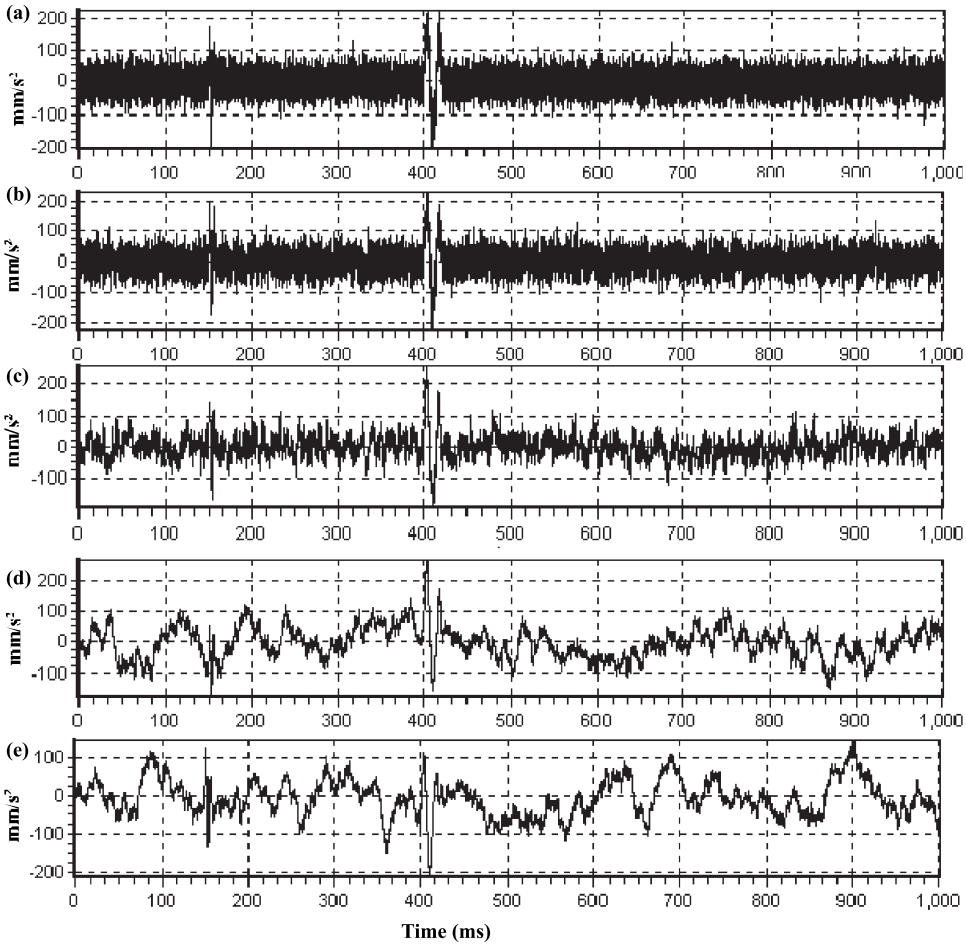

Figure 4
Superposition of wavelets illustrated in Figure 3 with varying ambient background noise.

Table 1

Gauss-Markov simulation parameters

Plot	Time constant (ms)	Variance (mm^2/s^4)
A	0.0001	1000
B	0.1	1000
C	1	1000
D	10	2000
E	20	2000

Figure 5 illustrates the autocorrelations of the Gauss-Markov noise processes illustrated in Figure 4(a) to (e). Figure 5 also illustrates the best fit curves where the ambient noise *Time Constant* and *Variance* parameters were identical to those specified above.

In these simulations and subsequent results from processed real data, the MEDKF filter was specified as a three-state filter as described by eq. (26). The *P*-wave MEDKF filter parameters were first specified, results obtained and then the *S*-wave filter parameters were set and subsequent filter estimates derived. Had the MEDKF been set to a five-state filter (i.e., to incorporate both *P* wave and *S* wave into the same filter), it would have been possible to track both the *P* wave and *S* wave simultaneously. Alternatively, it would have been possible to track both the *P* wave and *S* wave with two three-state MEDKF filters running in parallel in software multitasking threads.

Referring to eqs. (16) and (26), the filter parameters set for the *P*-wave filter were $E[x_1(0)] = 0, E[x_2(0)] = 0$, and $E[x_3(0)] = z_0$, where z_0 is the data measurement at $t_0 = 0, \omega = 2\pi f$ where $f = 200$ Hz, and $P_0 = 0$ except for elements $P_0[1,1] = 80$, $P_0[2,2] = 80$, and $P_0[3,3] = 0$. The values set for x_0 and P_0 had no significant effect on the MEDKFs performance because it was found that the error covariance and filter gain values reached steady responses rapidly. The random walk Q value was set to 0.3, where $Q = q(t)*\Delta$ and $\sqrt{q(t)} \approx 77.5\,\mathrm{mm/s^2}$. The MEDKF responded robustly to variable Q values specified. In general, we have a more sluggish (low variability) response for lower Q values as compared to higher values.

The Gauss-Markov parameters of σ^2 and T_c (i.e., $1/\beta$) were derived adaptively and automatically from the recorded time series. The *S*-wave initial parameters were identical to those for the *P* wave except for the $f = 70$ Hz for the *S* wave. Since it is assumed that the ambient noise defined the time series error, the measurement error variance, $R(t)$, was specified at a fraction of the Gauss-Markov variance (i.e., $R(t) = \sigma^2(t)/1000$).

From our preliminary investigations, it was found that the best event detection state to track was the seismic wavelets amplitude (i.e., state x_2). Figure 6 illustrates the MEDKF results after tracking the *P* wavelet. As illustrated, we have obtained a dramatic improvement in the signal to noise ratio when comparing these results to the initial seismic time series outlined in Figure 4. Figure 7 shows the MEDKF

results after tracking the *S* wavelet. As with the *P* wavelet MEDKF results, an impressive improvement was recorded in the signal-to-noise ratio after the implementation of the MEDKF.

As mentioned in Section 2, the error covariance (Martix Ricatti) equation is a fundamental part of the KF formulation. The error covariance matrix provides for the determination of the Kalman gain and it quantifies the filter performance.

The continuous error covariance matrix for the MEDKF is defined as follows

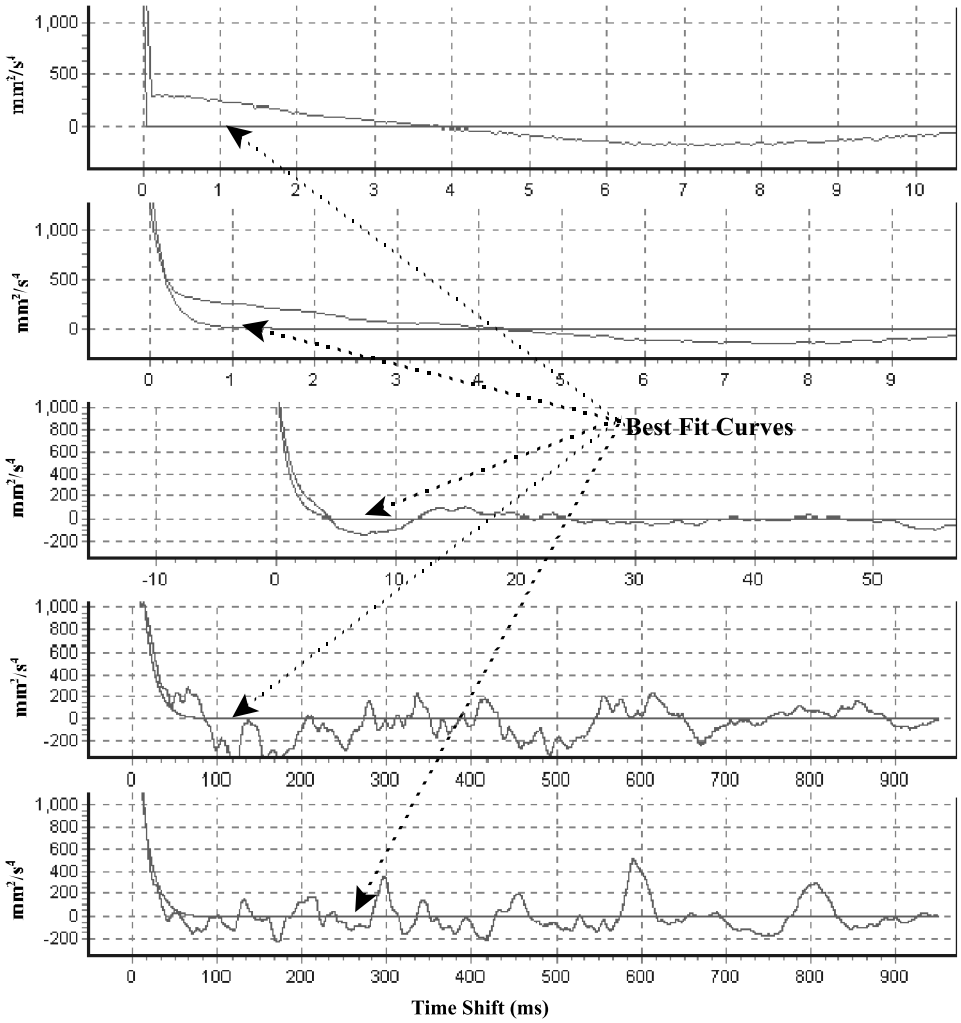

Figure 5
Applying a Gauss-Markov best fit to the simulated ambient noise autocorrelation.

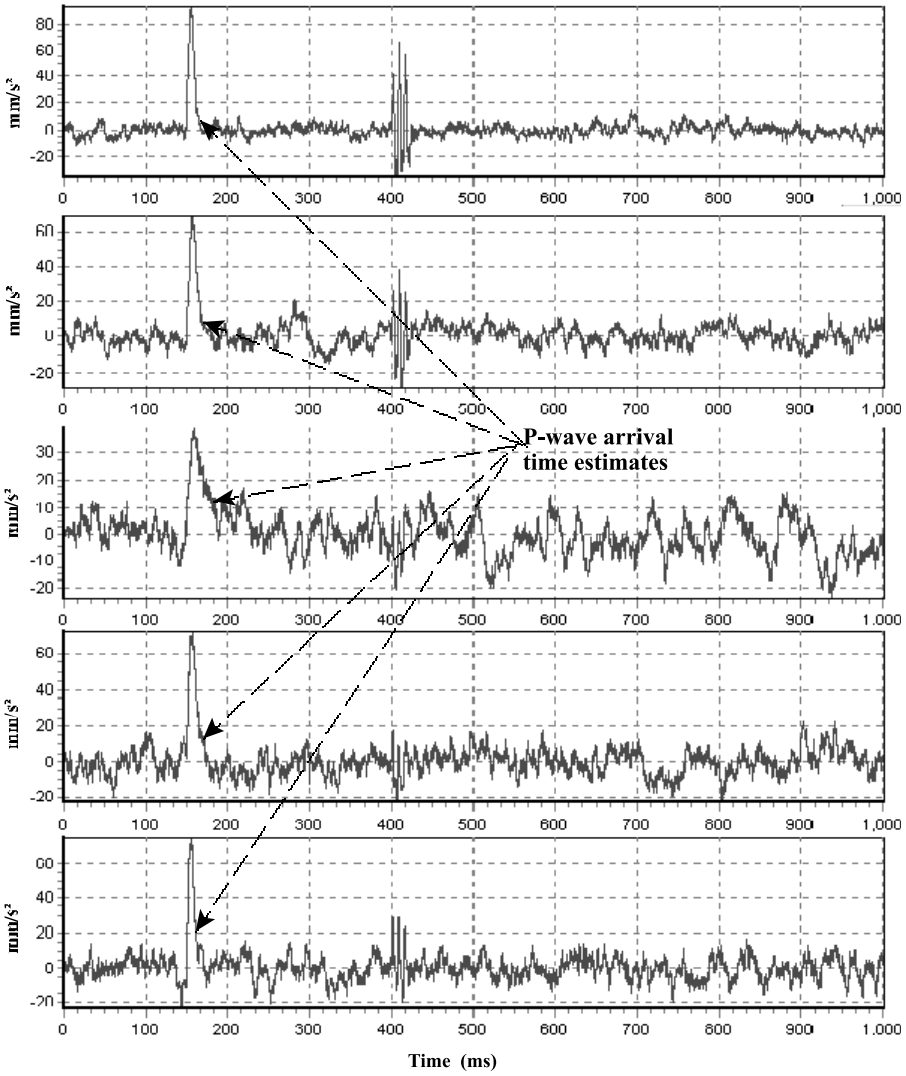

Figure 6
Kalman Filter results for the *P* wave. The seismic amplitudes (i.e., X_2) illustrated show excellent signal-to-noise ratio for the *P*-wave event detection.

$$\dot{P}(t) = \begin{bmatrix} 2P_{12}(t)\omega\cos(\omega t) & \bullet & \bullet \\ P_{22}(t)\omega\cos(\omega t) & Q & \bullet \\ P_{32}(t)\omega\cos(\omega t) - \beta P_{31}(t) & -\beta P_{32}(t) & -2\beta P_{33}(t) + \sigma^2(1 - e^{-(2\beta\Delta)}) \end{bmatrix} - B(t) \tag{28a}$$

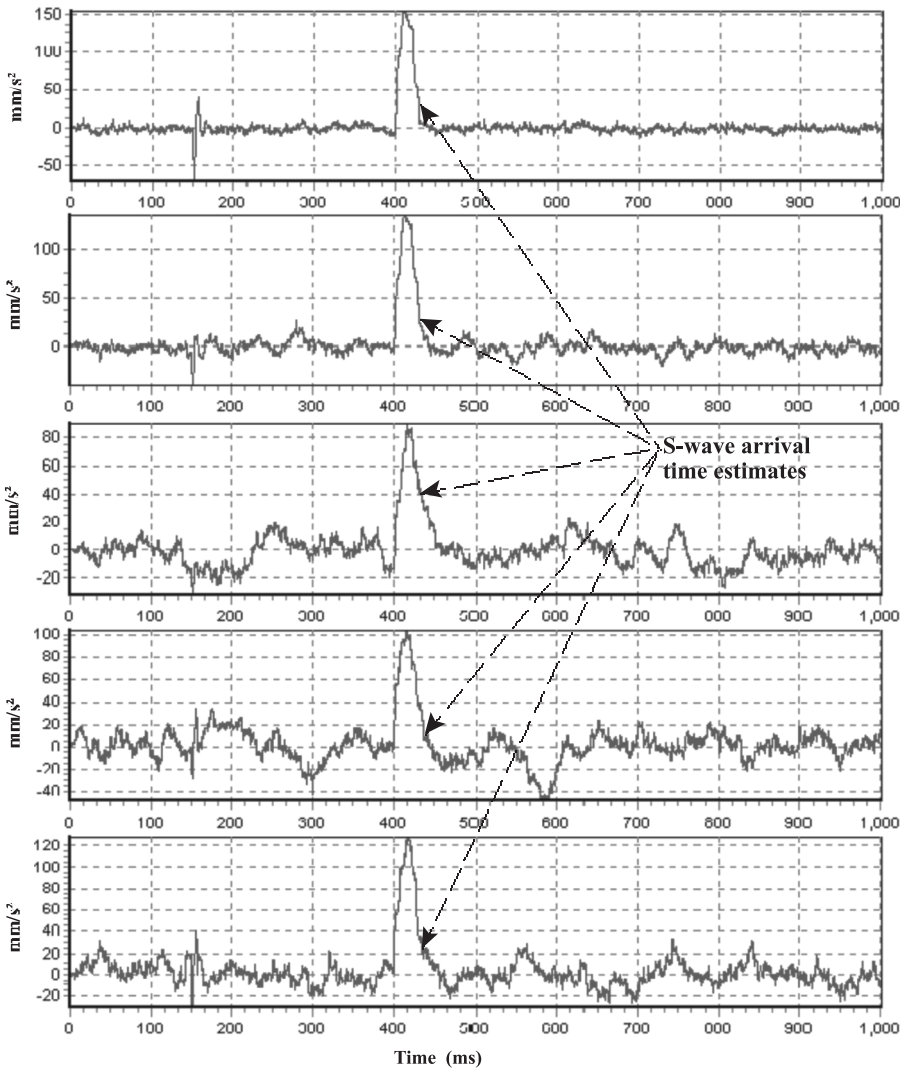

Figure 7
Kalman Filter results for the S wave. The seismic amplitudes (i.e., X_2) illustrated show excellent signal-to-noise ratio for the S-wave event detection.

where

$$B(t) = \begin{bmatrix} (P_{11}(t) + P_{13}(t))^2 & \bullet & \bullet \\ (P_{21}(t) + P_{23}(t))(P_{11}(t) + P_{31}(t)) & (P_{21}(t) + P_{23}(t))^2 & \bullet \\ (P_{31}(t) + P_{33}(t))(P_{11}(t) + P_{31}(t)) & (P_{31}(t) + P_{33}(t))(P_{12}(t) + P_{32}(t)) & (P_{31}(t) + P_{33}(t))^2 \end{bmatrix} \Big/ R(t) \quad . \tag{28b}$$

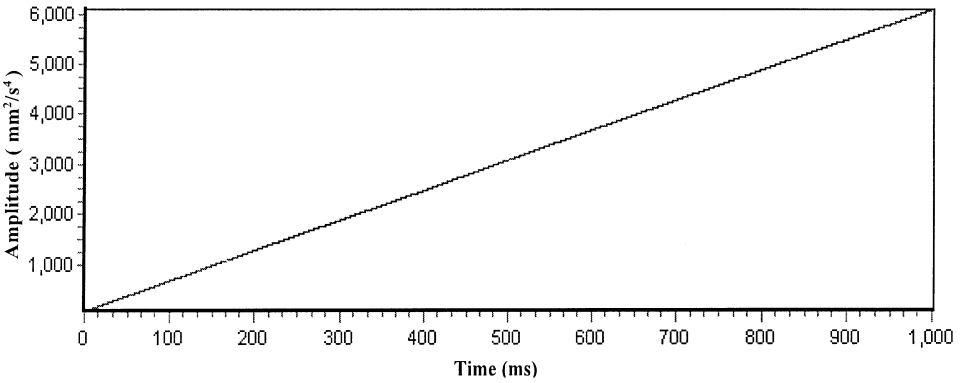

Figure 8
$P_{11}(k)$ response for $R(t) \Rightarrow \infty$ and MEDKF initial conditions.

For simplicity, the off diagonal terms in eqs. (28a) and (28b) have been omitted due to the symmetry of the error covariance matrix. The continuous error covariance for the amplitude estimate (i.e., state $x_2(t)$) is defined as

$$\dot{P}_{11}(t) = Q - (P_{21}(t) + P_{23}(t))^2 / R(t) \quad . \tag{29}$$

We see from eq. (29), that if there is a high measurement (i.e., $R(t) \Rightarrow \infty) P_{11}(t)$ would grow linearly at a rate specified by the random walk variance Q. Figure 8 illustrates the discrete $P_{11}(k)$ value with a very high $R(t)$ specification and our initially specified Q value of 0.3. The fact that accurate measurements are utilized (i.e., low $R(t)$), allows the MEDKF to constrain our error covariance estimates and bring them to steady-state responses.

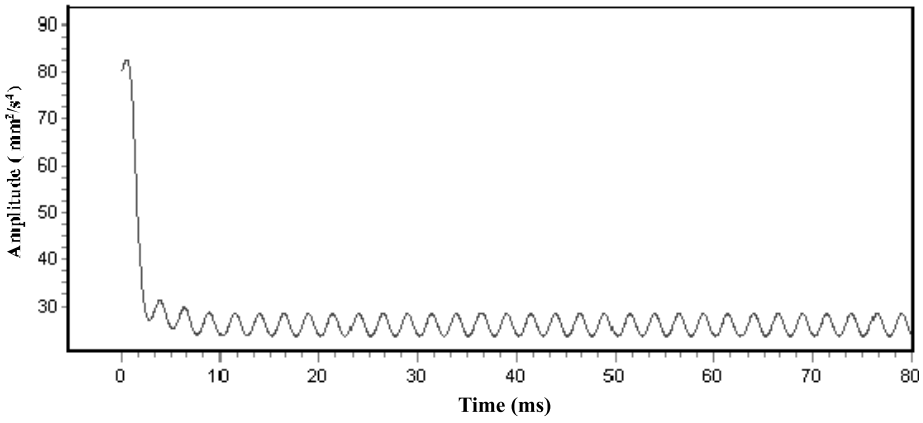

Figure 9
$P_{11}(k)$ response for $R(t) = \sigma^2(t)/1000$ and MEDKF initial conditions.

In general terms, the error covariance estimate $P_{11}(t)$ is directly proportional to Q, σ, and β, and inversely proportional to $R(t)$. In addition, because term $P_{21}(t)$ is a function of $\cos^2(\omega t)$, we would expect $P_{11}(t)$ to have components of oscillation at $2^*\omega$ where $\omega = 2\pi f$. Figure 9 illustrates the $P_{11}(k)$ responses for the P-wave estimate for test case A. As is shown, the error covariance estimate, $P_{11}(k)$, behaves as expected where it reaches a steady response rapidly from the initially specified $P_{11}(0)$. $P_{11}(k)$ then oscillates at the steady response rate of $2^*\omega$ or $f = 400$ Hz. It is also important to bear in mind that P_{11} reflects uncertainty of both the A_0 and t_0 parameters in eq. (21).

3.2 Processing Real Data

The data presented in this paper were obtained from some of the microseismic installations Weir-Jones Engineering Consultants has commissioned at heavy oil extraction operations in Northern Alberta. Earlier work in this region has been described by other authors (TALEBI *et al.*, 1998).

The Cold Lake area is located in Northern Alberta, Canada. Extensive, heavy oil reserves underlie the area. The oil sands occur in the Mannville Group of Lower Cretaceous age and range from 305 m to 610 m below surface. The primary reservoir is the Clearwater formation at an average depth of 457 m. The sand in the Clearwater is laterally and vertically continuous and pay thickness ranges from 15 m to 49 m. The reservoir has 11 billion m^3 of bitumen in place.

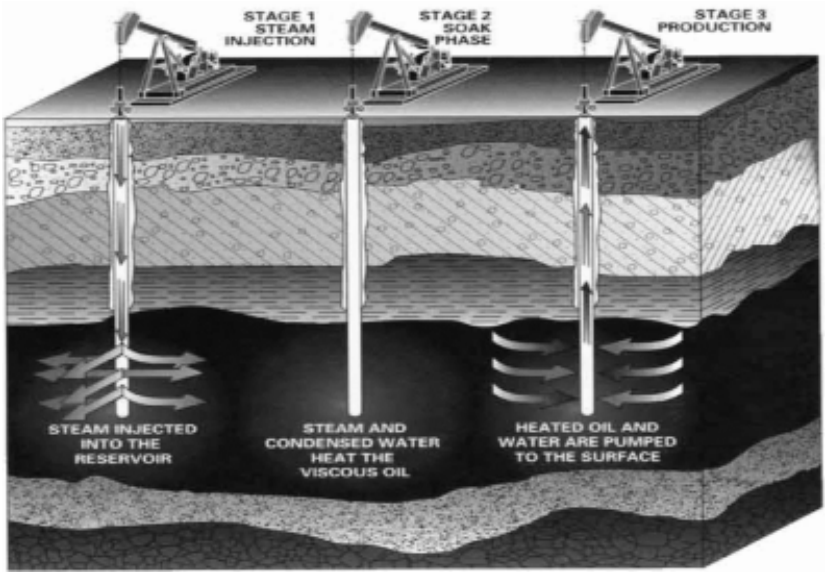

Figure 10
Typical steam injection mechanism in Northern Alberta.

The Clearwater sand is an unconsolidated clean sand with porosities between 30% and 35% and an average bitumen saturation of 70%. The absolute permeability ranges from $0.5 \times 10^{-12}\,m^2$ to $2 \times 10^{-12}\,m^2$ and viscosity reaches 150,000 cp. Initial reservoir conditions are 3 °C and 3 MPa. Figure 10 illustrates a typical steam injection mechanism in which there is pancake stratigraphy which is defined as follows:

Formation top	Depth (m)
Surface	0
Colorado Shales	149
Grand Rapids	319
Clearwater	432
McMurray	485

Overlying the Clearwater is the Grand Rapids formation, which consists of sands and shales. Above this is the Colorado Group of Upper Cretaceous age. It consists of marine shales that are impervious and separate the oil sands from the glacial tills near surface. Since most of the oil sands are immobile, additional heat and pressure are required to recover the bitumen. Three main processes used are cyclic steam stimulation, steam drive and steam assisted gravity drainage. A detailed technical description of the microseismic monitoring equipment and geophone array installation was presented by TALEBI (1998).

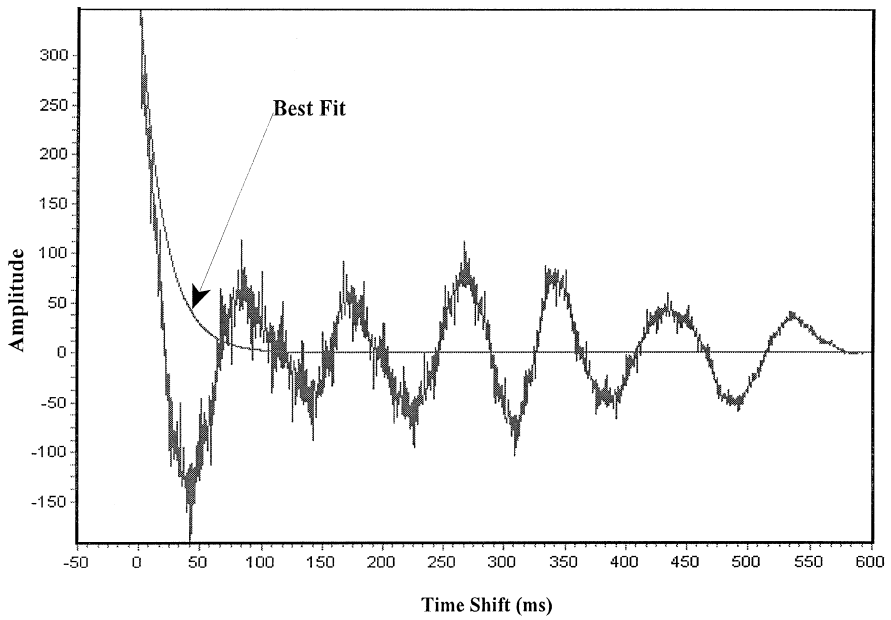

Figure 11
Autocorrelation calculated from the seismic time series presented in Figure 12 (a). The best fit parameters are $\sigma^2 = 350\,mm^2/s^2$ and $T_c = 20\,ms$.

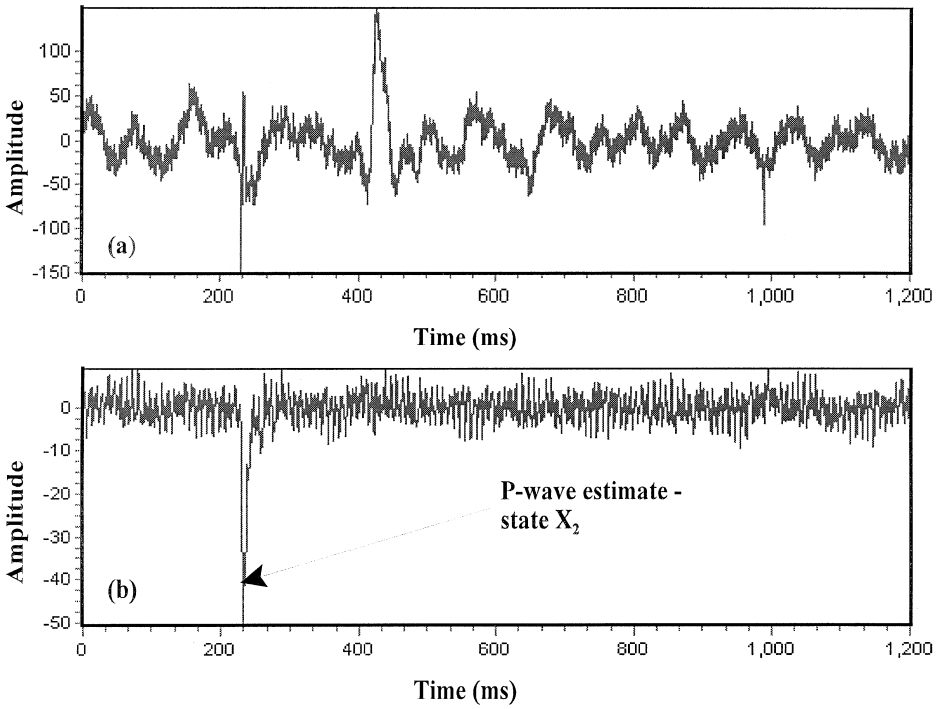

Figure 12
Input seismic trace (a), and the result based on the implementation of the Kalman Filter (b), as was outlined in section 2 ($f = 185\,\text{Hz}$ for the P wave).

The data analysed in this paper were obtained using proprietary geophone arrays specifically developed by the authors for these applications. The geophone arrays consist of multiple sensing elements arranged on orthogonal axes. The arrays have a natural frequency of 10 Hz, are damped at 70% of critical, and have a bandwidth from 8 to 900 Hz.

Figure 11 illustrates the autocorrelation function of the seismic trace presented in Figure 12(a). This autocorrelation was calculated by windowing on the portion of data 600 ms and 1200 ms. The exponentially correlated process illustrated in Figure 11 was fitted with the parameters $\sigma^2 = 350\,\text{mm}^2/\text{s}^2$, and $T_c = 20$ ms. Figure 12(b) illustrates the results of implementing the MEDKF on the seismic trace presented in Figure 12(a) with the parameters specified by fitting the autocorrelation presented in Figure 11 and the dominant frequency set to 18.5 Hz for the P-wave response. The remaining MEDKF initial filter parameters were set in an identical manner to those specified in the previously outlined simulated results. As is shown in Figure 12(b), there has been a dramatic improvement in the signal to noise increase after implementation of the MEDKF.

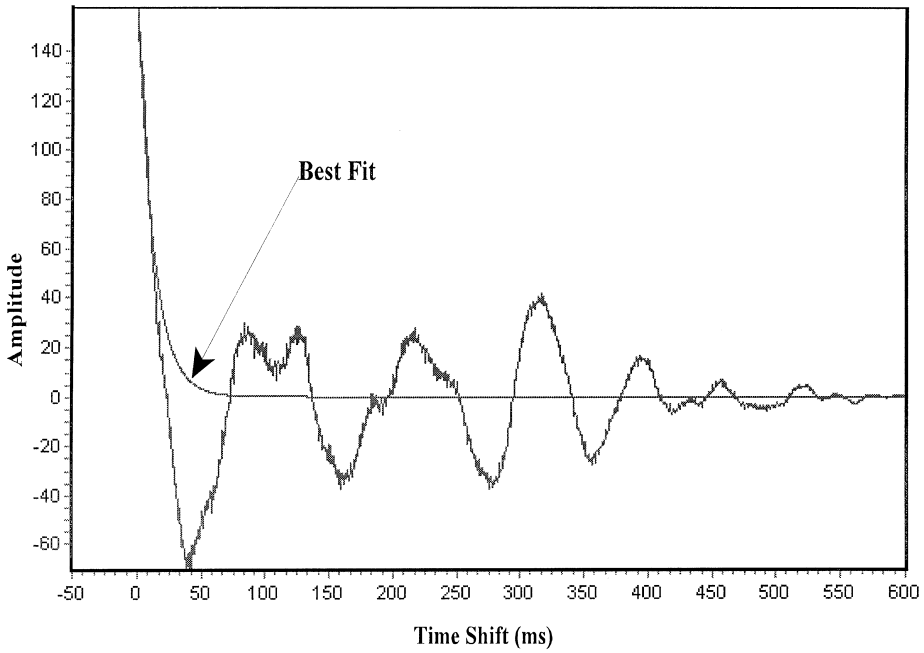

Figure 13
Autocorrelation calculated from the seismic time series presented in Figure 14(a). The best fit parameters are $\sigma^2 = 157\,\mathrm{mm}^2/\mathrm{s}^2$ and $T_c = 13\,\mathrm{ms}$.

The next set of data illustrates the MEDKF's abilitty to identify the *P*-wave and *S*-wave responses from the time series in real time. Figure 13 shows the autocorrelation function of the seismic trace presented in Figure 14(a). This autocorrelation was again calculated by windowing on the portion of data between 600 ms and 1200 ms. The Gauss-Markov noise process illustrated in Figure 13 was fitted with the parameters $\sigma^2 = 157\,\mathrm{mm}^2/\mathrm{s}^2$, $T_c = 20\,\mathrm{ms}$. In this analysis the frequency was set to 185 Hz for the *P*-wave response and a frequency of 30 Hz for the *S*-wave response. Figure 14(b) and 14(c) illustrate the results after filtering. Similarly to Figure 12(b), we again obtain excellent results where the *P*-wave and *S*-wave arrivals are clearly identified.

Figure 15(a) illustrates a time series where it is very difficult to identify the *P* wavelet visually, let alone automatically. In this test case the dominant frequency was set to 170 Hz for the *P*-wave response. The exponentially correlated noise process illustrated was fitted with the parameters $\sigma^2 = 7.7\,\mathrm{mm}^2/\mathrm{s}^2$, and $T_c = 20\,\mathrm{m\,sec}$. Figure 15(b) illustrates the filtered results where the *P*-wavelet response has been more clearly identified.

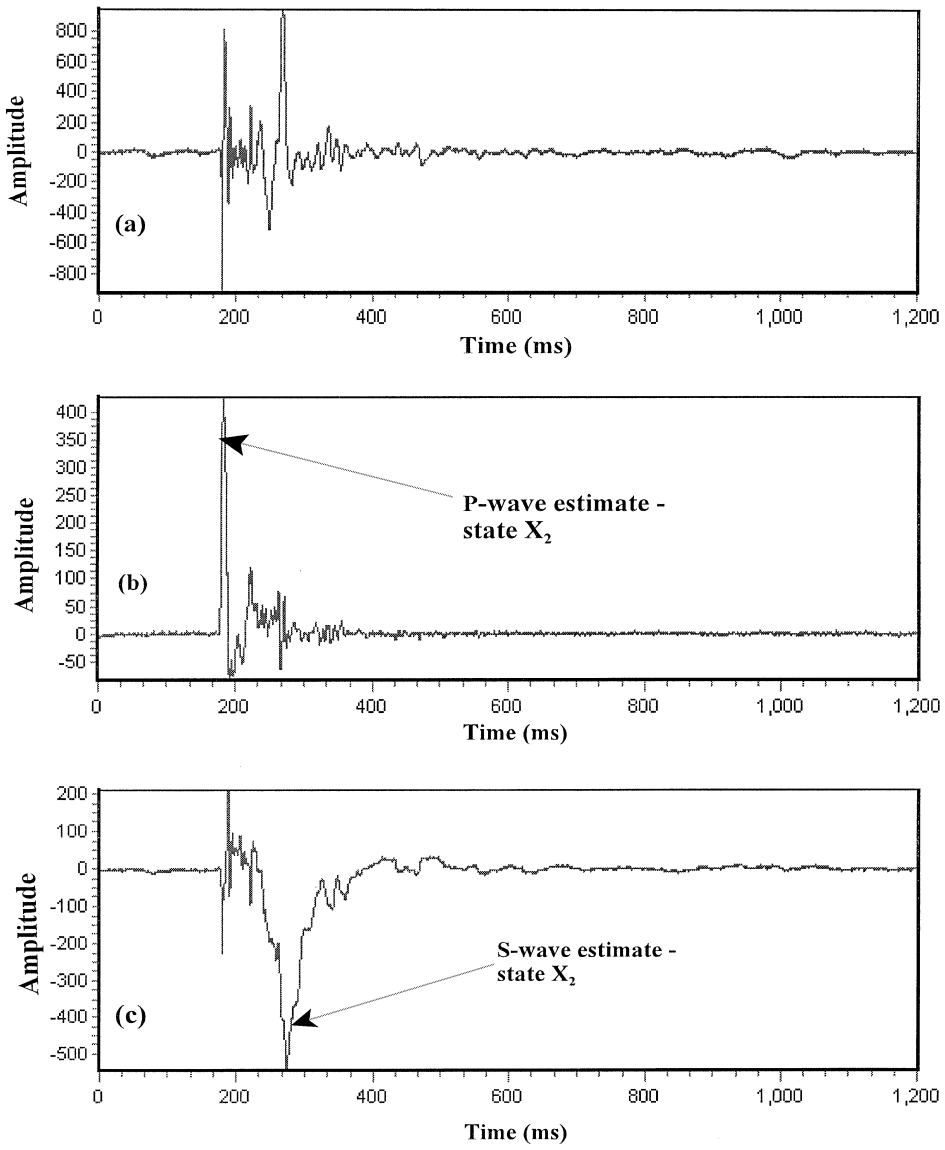

Figure 14
Input seismic trace (a); Kalman Filter *P*-wave arrival time estimation results ($f = 185$ Hz) (b); Kalman Filter *S*-wave arrival time estimation results ($f = 30$ Hz) (c).

4. Conclusions

In microseismic monitoring programs it is important to have reliable event triggering and source parameter characterization. Poorly defined passive microseis-

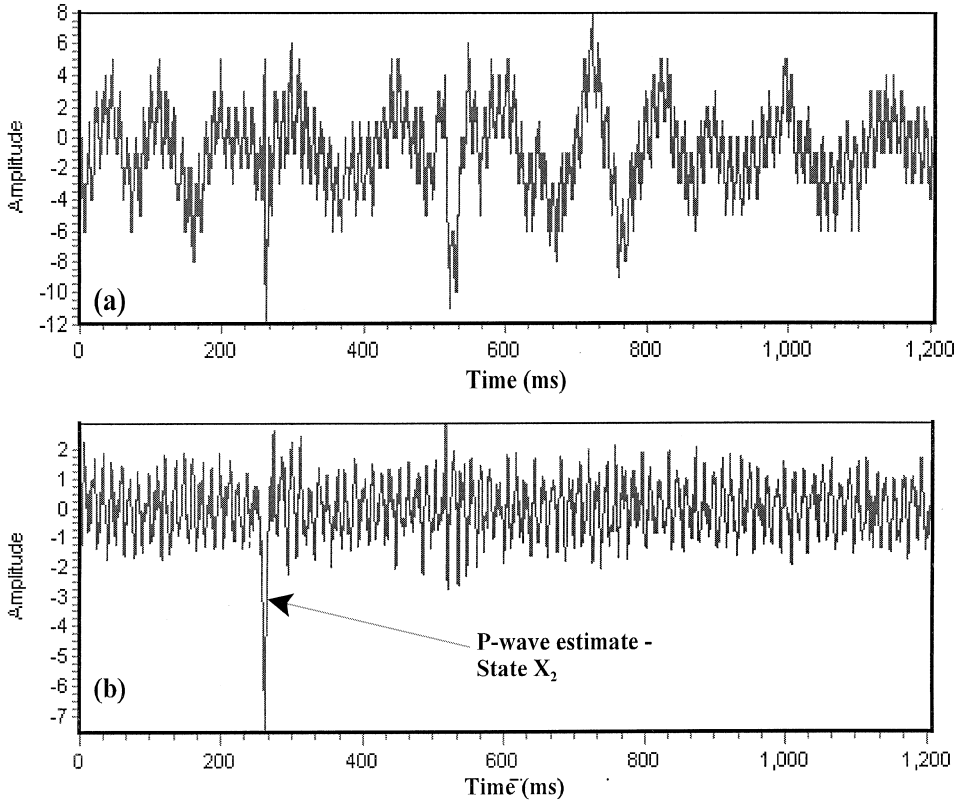

Figure 15
Input seismic trace (a), and Kalman Filter *P*-wave arrival time estimation results ($f = 170\,\text{Hz}$, $\sigma^2 = 7.7\,\text{mm}^2/\text{s}^2$, and $T_c = 20\,\text{ms}$).

mic triggering algorithms tend to acquire substantial amounts of data which demand extensive post-processing manipulation; they also increase the work and reduce the efficiency of the personnel operating the systems. This paper presented a real-time Kalman Filter which modelled the background noise as a Gauss-Markov process and the seismic wavelet as a periodic process with a random walk initial amplitude. The filter allows for online processing and circumvents many of the problems associated with frequency domain filters.

Both simulated signals and seismic data acquired from passive microseismic installations in Northern Alberta were analysed and the results evaluated in terms of the improvement in signal-to-noise ratio. The results are very encouraging; there is a substantial improvement in signal-to-noise ratio after implementation of the Kalman Filter. For example, for the simulated data presented, there is an approximate 12-old increase in the signal-to-noise ratio as a result of the post-processing. For the

processed real data, the signal-to-noise ratio is enhanced by approximately six times (i.e., Fig. 12).

The authors' ultimate objective is to provide a system which offers microseismic system operators a reliable and cost-effective procedure which can process microseismic data in real-time and provide accurate event locations with a reduction in the amount of system operator intervention.

Acknowledgements

The authors would like to thank Robert Rasmusens for his software engineering assistance.

References

Bayless, J. W. and Brigham, E. D. (1970), *Application of the Kalman Filter to Continuous Signal Restoration*, Geophysics *35*, 2–23.

Baziw, E. J. (1993), *Digital Filtering Techniques for Interpreting Seismic Cone Data*, ASCE. J. Geotech. Engin. *119*(6), 998–1018.

Baziw, E. J. (1988), *Applications of Digital Filtering Techniques for Reducing and Analysing In-Situ Seismic Time Series*, MASc Thesis, Dept. of Civil Engineering, University of British Columbia, Vancouver, BC.

Baziw, E. J. (1994), *Dead Reckoning/Target Tracking in a ECDIS Environment*, Institute of Navigation's National Technical Meeting, San Diego California, January 26, 747–756.

Gelb, A., *Applied Optimal Estimation*, (4th edition, MIT Press, Cambridge, Mass. 1978).

Kanasewich, E. R., *Time Sequence Analysis* (3rd edition, The University of Alberta Press 1981), 230 pp.

Lear, W. M., *Kalman Filtering Techniques* (National Aeronautics and Space Administration Publication, Mission Planning and Analysis Division, No. JSC-20688 1985), pp. 172–176, 321–335.

Mendel, J. M., *Optimal Seismic Deconvolution An Estimation-Based Approach*, (1st Edition, Academic Press, 1983).

Mendel, J. M., *Lessons in Estimation Theory for Signal Processing, Communications, and Control* (Prentice Hall PTR, Englewood Cliffs, NJ, 1995).

Sheriff, R. E. and Geldart, L. P., *Exploration Seismology* Volume 1 (2nd edition, Cambridge University Press, Cambridge, UK 1982), 55 pp.

Talebi, S., Ge, M., Rochon, P., and Mottahed, P. (1994), *Analysis of Induced Seismicity in a Hard-rock Mine in the Sudbury Basin*, Ontario, Canada, Proceedings of the 1st North American Rock Mechanics Symposium, the University of Texas at Austin, June 1–3, 937–944.

Talebi, S., Nechtschein, S., and Boone, T. J. (1998), *Seismicity and Casing Failures Due to Steam Stimulation in Oil Sands*, Pure appl. geophys. *153*, 219–233.

(Received July 20, 2000, revised January 10, 2001, accepted January 11, 2001)